



Triboelectric-Based Film-Type Soft Robot Driven via Low-Frequency Mechanical Stimuli

Sungho Ji¹ · Jaehee Shin¹ · Jiyoung Yoon² · Jung-Hwan Youn³ · Jihyeong Ma³ · Ki-Uk Kyung³ · Duck Hwan Kim⁴ · Hanchul Cho⁵ · Jinhyoung Park¹

Received: 7 April 2022 / Revised: 29 September 2022 / Accepted: 7 October 2022 / Published online: 15 November 2022
© The Author(s), under exclusive licence to Korean Society for Precision Engineering 2022

Abstract

Triboelectric nanogenerators (TENGs) have received considerable attention owing to their ability to harvest energy from the environment. They can be effectively used as a self-generating power source to drive low-power devices. Compared with other energy harvesting technologies, the energy conversion efficiency is much higher, but the current output is low—only enough to drive an existing rotor-type motor. In this study, we designed a film-type soft robot that can produce high-voltage, low-power, triboelectric output without using a motor. Polyvinylidene fluoride (PVDF) film was used as the actuator for the soft robot. We designed a resonance structure to increase the movement of the soft robot driven by low-frequency triboelectric output. A driving test was performed by simulating the shape of butterfly wings and an inch-worm. When the butterfly-shaped PVDF film robot simulated the flapping motion of wings using the resonance structure parameter design, it was able to generate 2.5 times greater movement than the model without the resonance structure. In addition, the artificial inch-worm soft robot optimized for the TENG input was fabricated by applying the parameter design method to the PVDF film. We developed and tested a self-powered, intelligent soft robot that can be driven by low-frequency mechanical stimuli. This study can help extend the application of triboelectric generators.

Keywords Triboelectric nanogenerator · Soft robot · Polyvinylidene fluoride film actuator · Artificial insect robot · High voltage application

1 Introduction

Modern soft robots are designed using film-type actuators powered by flexible bending actuation. Film-type actuators include piezoelectric materials [1–4], electroactive polymers [3, 5, 6], and artificial muscle materials [7]. The piezoelectric-type actuator was primarily used as a film-type vibration sensor utilizing piezoelectric effects. Conversely, if an electric signal is input to the piezoelectric material, it can bend; thus, it can be used as an actuator. Piezoelectric material film-type actuators are primarily used for haptic vibration sensor and film-type speakers. Recently, a study was conducted to understand the movement of insects through natural imitation (biomimetic) using a piezoelectric material film-type actuator [8]. Although the piezoelectric material film actuator has fast response speed, light weight, and excellent stability, its application is limited owing to its high driving voltage requirement.

The triboelectric nanogenerator (TENG), first introduced by Fan et al. in 2012, is characterized by high output and

✉ Jinhyoung Park
jhpark98@koreatech.ac.kr

¹ School of Mechatronics Engineering, Korea University of Technology and Education, Cheonan 31253, Republic of Korea

² Mechatronics Technology Convergence R and D Group, Korea Institute of Industrial Technology (KITECH), 320 Techno Sunhwan-Ro, Yuga-Eup, Dalseong-Gun, Daegu 42994, Republic of Korea

³ Department of Mechanical Engineering, Korea Advanced Institute of Science and Technology, Daejeon 34141, Republic of Korea

⁴ Robot System Team, Samsung Research Seoul R and D Campus, Umyeong Dong 33, Seongchon-Gil, Seocho-Gu, Seoul 06765, Republic of Korea

⁵ Precision Mechanical Process and Control R and D Group, Korea Institute of Industrial Technology (KITECH), 42-7, Baeyang-Daero 804 Beon-Gil, Sansang-Gu, Busan 46938, Republic of Korea

energy conversion efficiency [9]. Applications using TENGs include low-power Internet of Things (IoT) devices [10–14], body implant devices [15–18], and self-generation power sources for wearable devices [15, 19–22]. In addition, a TENG develops a high voltage of 100 V or more and a low current output of about 10 μA [23–27]. To use a TENG to charge a small battery optimized at around 5 V, a significant amount of electrical conversion is required; hence, the efficiency is low. High voltage (HV) applications can use these TENG characteristics of high voltage and low current. An example of TENG HV application is the study of microplasma generation using a voltage of 5000 V [28]. Similarly, to drive the piezoelectric material film-type actuator, high voltage and low current are essential. If a TENG with high voltage and low current output characteristics is used, it is possible to supply power without going through an energy conversion process. Thus, it is possible to drive a piezoelectric film-type actuator using self-generation. As materials for actuators commonly used to manufacture soft robots, ceramic-based piezoelectric materials, shape memory alloys, and electroactive polymers are used. Although the shape memory alloy-based actuator has the advantage of large operating displacement and low operating voltage, its disadvantage is that it has a very slow response speed [29]. Electroactive polymers have advantages such as fast response speed and large operating displacement, but have the disadvantage of requiring a very large operating voltage [30]. Wang et al. fabricated a soft robot using an electroactive polymer based on a dielectric elastomer actuator (DEA), and it was reported that an input voltage of 4 kV is required to obtain a movement speed of 100 mm/s [31]. As described above, the soft robot manufactured using the electroactive polymer has a large operating displacement value, so it has the advantage of obtaining a fast moving speed. However, since it is manufactured in the form of a gel, the durability is not good and the driving force is weak compared to an actuator based on a piezoelectric material. Therefore, in this study, we propose a soft robot using a PVDF-based piezoelectric material film that is manufactured in the form of a film, has good durability, has excellent repeatability, and has a large driving force.

In this study, a piezoelectric film-type actuator was directly driven by converting external kinetic energy into electrical energy using a large-area TENG. TENGs, which are manufactured to supply power to actuators, can obtain optimal performance in the frequency band below 10 Hz. As this frequency band is present in the natural world, it is possible to collect electrical energy that can make the robot self-actualize. Applying the TENG technology to the soft robot allows for a simpler and cheaper structure because there is no need to configure equipment and application circuits such as the existing high voltage supply for power supply. Additionally, it is possible to manufacture it in an

eco-friendly manner because the waste energy is collected. However, the polyvinylidene fluoride (PVDF) actuator used to manufacture the body of the soft robot has a limitation in that the driving range is relatively small. To overcome this limitation, the resonant structure and optimal parameter design methods were applied to the butterfly and inch-worm robots, respectively. Through experimental analysis, we propose a design guide for the maximum moving speed of a soft robot that can operate through self-generation.

2 Material and Methods

2.1 Fabrication of the TENG

Figure 1 shows a schematic of an insect-simulating soft robot using the output performance of the TENG. First, we fabricated the TENG required to drive the PVDF film. The TENG consists of two parts. The first part was fabricated by inserting copper wool as an electrode into silicone rubber (Dragon Skin 10 NV) used as a negatively charged material. The main (part A) and hardener (part B) solutions were mixed in a 1:1 ratio. Subsequently, the mixture was stirred for 5 min using a spatula. Bubbles were generated when the mixture was stirred. It is possible to produce a porous structure with a large surface area if the silicone rubber is fabricated without removing the bubbles. Therefore, a separate degassing process was not used to remove the air bubbles. After pouring the prepared mixed solution into the mold, copper wool was added and the mold hardened at 40 °C for 2 h in a chamber (WiseVen, Won-60). The copper wool inserted inside the silicon rubber served as an electrode as well as improving the output performance by increasing the capacitance and dielectric constant. For the second part, an aluminum (Al) film used as a positive electrode was attached to a polymethyl methacrylate (PMMA) plate, and nitrile rubber, which is a positively charged material, was applied. We measured the contact potential difference (CPD) using Kelvin probe force microscopy (KPFM) to analyze the charging characteristics of the silicone rubber and nitrile rubber. The silicone rubber had a strong negative charge of -817 mV, and the nitrile rubber had a positive charge of 805 mV. A strong positively charged characteristic was observed [28]. The selection of an appropriate material is extremely important because the obtained output value increases as the difference in CPD values of materials with different charging characteristics increases.

2.2 Fabrication of the Soft Robot

Two types of PVDF film soft robots driven by TENGs were produced. The first was a soft robot that mimicked a butterfly. The flapping of a butterfly wing was simulated. The

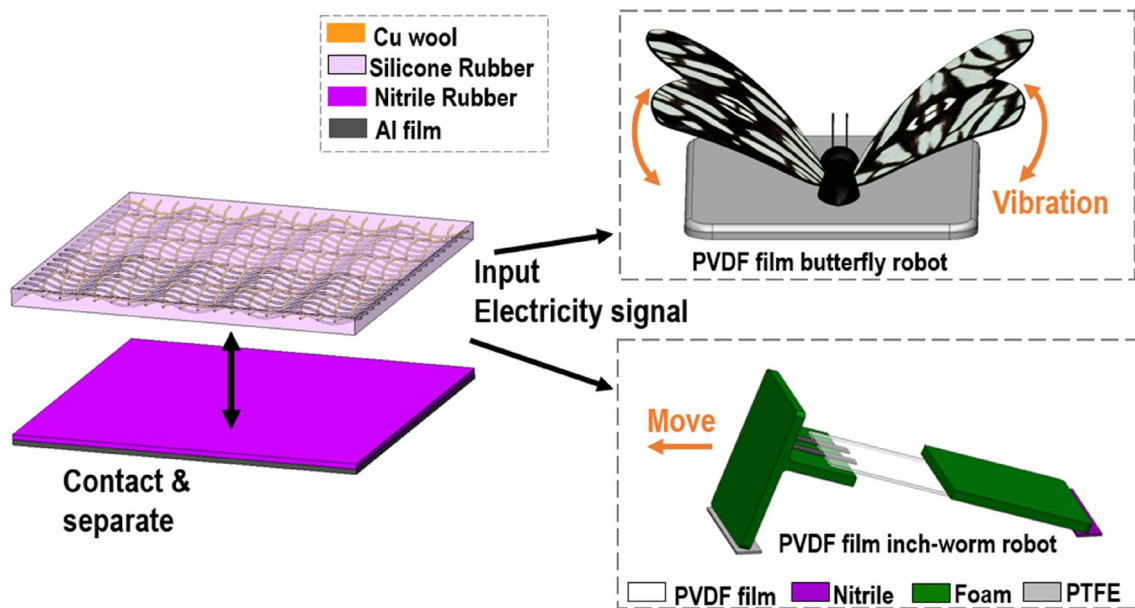


Fig. 1 Schematic of soft robots simulating insects fabricated using TENG electrical output and PVDF film actuator

butterfly soft robot was composed of a piezoelectric film, a paper with a butterfly wing pattern, and a mass for designing a resonance structure (Supplementary Fig. S1(a)). PVDF film (DT1-028 K, TE connectivity piezo film sensor) was used for the piezoelectric material film-type actuator, and Protection, antigen (Ag) paste, PVDF, Ag paste, and Protection were stacked on top of each other to make five layers. The resonance effect was induced by attaching a butterfly wing to the end of the PVDF film and a mass was added on the back of the butterfly wing. By applying the resonance structure design, the small movement (characteristics of the PVDF film) could be amplified.

The second was an inch-worm type soft robot that mimicked the movement of an inch-worm. The inch-worm robot used PVDF film as an actuator. In addition, we used the optimal parameter design method to create the forward movement according to the TENG output value. Five parameters were set for optimal parameter design (Supplementary Fig. S1(b)). We adjusted the parameters to derive the maximum speed of the forward movement. We analyzed the movement speed according to each parameter. For the forward movement of the inch-worm soft robot, materials with different friction factors were applied to the front and rear pads. The rear pad served to push the film-type robot to advance. Therefore, a nitrile rubber pad with a large friction factor was used. On the other hand, polytetrafluoroethylene (PTFE) film material, a material with a small friction factor, was used for the front pad to slide forward after the rear pad pushed and after a half cycle. The friction factors of the material applied as the pad were

0.7 and 0.05, respectively. Experimental results based on other parameters are detailed in the results section.

2.3 TENG Experiment Configuration

A linear motor (Linmot, custom made), oscilloscope (TBS 2072, Tektronix, Oregon, U.S.A.), current amplifier (DLPCA-200, Femto, Berlin, Germany), and high voltage probe (P5100A, Tektronix, Oregon, U.S.A.) were used to measure the electrical output characteristics of the TENG. A control PC was used to control the experimental device. The frequency of the linear motor was set to 4 Hz by the Linmot software in the control PC.

In the fabricated TENG, the positively charged material part was attached to the striking plate of the linear motor, and the negatively charged material part was folded and fixed in a circular cylinder shape considering the effective contact area and then placed on the base part of the linear motor. A laser displacement sensor (DTS-050-10, MTI co., U.S.A.) was used to measure the displacement of the butterfly wings. A large-area TENG output performance tester (sub series, SPG) was used to control the inch-worm soft robot.

2.4 Simulation Method of TENG Electromagnetic Field Analysis

COMSOL Multiphysics was used to analyze the strength of the electromagnetic field generated as the distance between the triboelectric layers constituting the TENG was reduced.

A tetrahedral element was used for the element type, an Al film was applied to the Ground as a boundary condition, and the Terminal voltage was applied to the interface between the silicone rubber and metal wool for analysis. In addition, modal analysis was performed using MESHFREE software to analyze the natural frequency of the butterfly wings. A fixed condition was given to one end of the shape as a boundary condition, and the frequency generated in MODE 1 was analyzed by applying the butterfly wings and coins attached to the opposite side in a concentrated manner; here, the arch-shaped beam, mass coin, and paper were rigidly linked and behaved together.

3 Results and Discussion

3.1 TENG Working Principle and Mechanism

In this study, the TENG fabricated to drive the PVDF film operated in the vertical contact-separation mode. PVDF film has fast response speed, light weight, and excellent stability, but requires a high driving voltage. By using the characteristics of high voltage and low current of the TENG directly as a power source, it is possible to supply power effectively

without any loss caused by electrical conversion. Therefore, it is important to increase the electrical output value generated by the TENG. Typically, methods such as increasing the surface area, surface charge density of the material, and kinetic energy rate or increasing the effective contact area through a surface etching process are used to improve the output performance. In this study, silicone rubber (a porous material with a high surface charge density) was used to produce a large area for the TENG to obtain a high output voltage. The size of the fabricated TENG was $400 \times 250 \times 5$ (mm^3).

Figure 2(a) depicts the mechanism of charge transfer that occurs when the TENG operates in the contact-separation mode. The initial state is before contact (Fig. 2(a (i))). The external force acting on the TENG makes perfect contact (Fig. 2(a (iii))), electrical neutrality between the silicone rubber and nitrile rubber is maintained, and no charge transfer occurs. In the pressing state (Fig. 2(a (ii))), in which the distance between the two parts of the TENG is shortened due to the action of an external force, the electrons of the aluminum film attached to the nitrile rubber move into the silicone rubber to maintain an electrically neutral state. Electric charge is transferred to the copper wool. Conversely, when the applied external force is released, the separation of

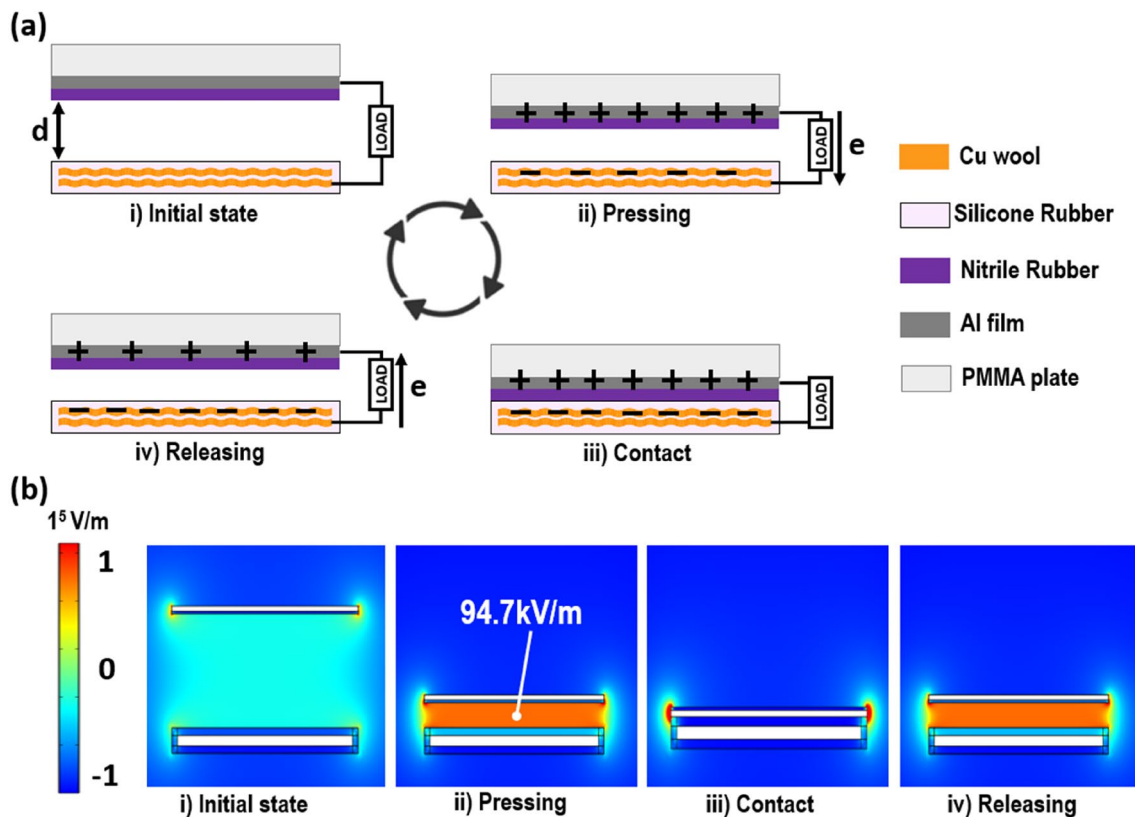


Fig. 2 Mechanism of contact-separation mode TENG and electric field simulation using COMSOL Multiphysics; **a** charge transfer mechanism that occurs in the contact-separation process; **b** simulation of electric field change occurring during contact-separation process

the two parts of the TENG begins (Fig. 2(a (iv))); the charge transfers back from the copper wool to the aluminum film. This charge transfer mechanism is explained by the coupling of triboelectric charging and electrostatic induction. In addition, we performed electric field analysis based on the distance between the two parts using COMSOL Multiphysics (Fig. 2(b)). It was confirmed that the strength of the electric field increases as the distance between the two parts increases, and electric charge transfer does not occur between the two parts because the field is balanced when the parts are in contact. For the analysis of the electric field of the TENG generated in the contact and separation mode, two parts were constituted to construct the COMSOL simulation. To proceed with the simulation, the mesh type was manufactured with a tetrahedral element. Among the boundary conditions, the ground was applied to the Al film, and the terminal voltage was applied to the interface between silicone rubber and metal wool by 500 V to analyze the strength of the electric field that occurs as the distance between parts changes Table 1.

3.2 Electric Properties of TENG and Resonant Structure Design

A common disadvantage of PVDF films is the extremely high driving voltage. We used a TENG with high voltage characteristics, and the output performance of the TENG was controlled and measured through a linear motor setup (Fig. 3(a)). By adjusting the stroke length and stroke time of the linear motor, the TENG was hit with a frequency of 4 Hz. The dimension of the TENG specimen used in the experiment is $300 \times 200 \times 3t$ (mm), and the test was conducted by rolling the fabricated specimen in a circular cylinder shape and hitting it using a linear motor. Since the rolling type TENG specimen can effectively increase the effective contact area, it is a method to improve the output performance (Fig. 3(b)). In order to optimize the operation of the butterfly wing mimicking soft robot, the TENG shape was classified into two and the output performance was analyzed. It is suitable that the waveform of the output voltage has a wide shape to make a continuous

fluttering motion by supplying power stably. Therefore, by rolling the sheet-type TENG in a cylindrical shape, the contact area was improved due to the additional internal contact, and a wider output waveform was obtained than the output waveform in the form of a single peak (Fig. 3(c) and (d)). In addition, the deformation characteristics and output performance of the rolling type TENG according to the force applied to the TENG were analyzed (Figs. S2 and S3). PVDF film is an actuator film that responds to a voltage in both directions (positive and negative). Therefore, we did not configure a rectifier circuit to reverse the output generated by the TENG. Normally, many electrical conversion circuits are configured to apply the electrical output of the TENG to the application, but the efficiency is greatly reduced in the conversion process. In this study, effective power supply is possible because the electric output is applied directly to the PVDF film without using a rectifier. We tested the output power levels by changing the external impedance value using a variable resistor. The highest output power occurred at 40 M Ω (Fig. 3(e)) When the PVDF film was driven using the output performance obtained through the experiment, it was observed that the operating displacement of the film was small.

In order to analyze the driving displacement of the PVDF film according to the output performance of the TENG, an experiment was conducted using cantilever structure. The range of force applied to the TENG is 2 N, 4 N, 6 N, 8 N, 10 N. When 10 N is applied, the effective contact area increases, so the highest output performance values of 740 V and 17 μ A can be obtained. In addition, as the TENG output applied to the PVDF film increases, it can be seen that the driving displacement of the PVDF film also increases (Fig. 3f–h).

In order to drive the soft robot effectively, it is essential to design it such that it shows a large displacement even with a small input. Therefore, we carried out a resonance structure parameter design to generate a resonance phenomenon from external vibration. The following equation was used to calculate the natural frequency of the resonant structure.

$$f(\text{HZ}) = \frac{1}{2\pi} \sqrt{\frac{k}{m}} = \frac{1}{2\pi} \sqrt{\frac{3EI}{ml^3}}, \quad (1)$$

where f is the natural frequency, k is the spring constant, and m is the weight. E is the Young's Modulus of the bar, l is the length of the bar, and I is the moment of inertia. The bar used in the design of the resonance structure was made of polyethylene terephthalate (PET), offering high elasticity and resilience. We designed the mass (coin) with weight 1.23 g and length 50 mm. The resonant frequency was set at 4 Hz (a value between 1 and 10 Hz that exists in nature). We simulated the flapping motion of a butterfly

Table 1 Simulation condition

Symbol	Name	Quantity	Unit
ϵ_{r1}	Silicone rubber Relative permittivity	3.5	–
ϵ_{r2}	Nitrile rubber relative permittivity	8	–
–	Ground (Al film)	–	–
V	Terminal voltage (Silicone rubber)	500	V

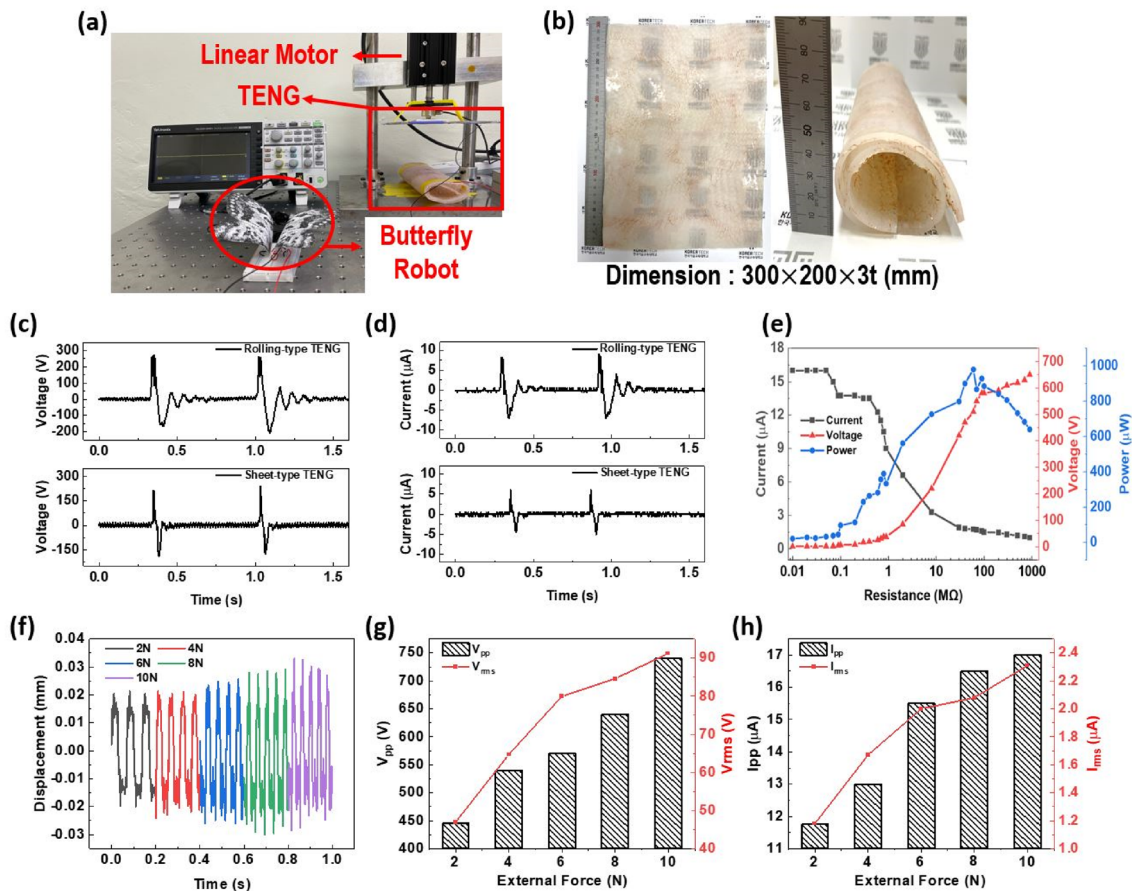


Fig. 3 TENG output performance evaluation; **a** experimental setup consisting of linear motor and control PC for quantitative output performance evaluation; **b** dimension of TENG specimen; **c** comparison of output voltage waveforms generated by the two types of TENG; **d** comparison of output current waveforms **e** output performance test at

varying external impedance; **f** driving displacement test of cantilever structure PVDF film according to TENG output performance; **g** output voltage according to external force; **h** output current according to external force

wing (movie S1) using the resonant structure parameter design (amplifying a small displacement value into a large displacement).

Figure 4(a) is a laser displacement sensor experimental setup for measuring the displacement of a butterfly wing driven by a TENG. A laser displacement sensor was connected to the control PC to measure the displacement of the flapping wing. In addition, a modal analysis was performed using MESHFREE software (Fig. 4(b)) to confirm the natural frequency of the butterfly wing calculated through Eq. (1). We assumed, for the experiment, that one end of the cantilever-shaped bar was fixed to the floor, and the mass coin and wing shape attached to the bar were treated as concentrated masses and excluded from the analysis. The modal analysis confirmed that MODE 1 has a natural frequency of about 4.029 Hz.

To confirm that the output performance meets the resonance condition, the frequency response of the TENG output was verified through Fast Fourier Transform (FFT). We

confirmed that the magnitude of the output was the largest at about 4 Hz (Fig. 4(c)). The electric output generated by the TENG was input to the butterfly soft robot as a power source. The difference in displacement generated according to the electric output was measured. When a voltage is input in the anode direction, the PVDF film bends upward to show a displacement of approximately 0.8 mm. The PVDF film bends downward and shows a displacement of about -0.8 mm (Fig. 4(d)) when a voltage is input in the cathode direction. To confirm the validity of the resonance structure parameter design used for the butterfly wing, we carried out a comparative analysis using a butterfly wing without a resonance structure. When the same TENG was used as a power source, the butterfly wing, without a resonance structure, showed a displacement of about ± 0.3 mm. The butterfly wing with the resonance structure design generated a displacement of ± 0.8 mm, which represents a 2.5-times increase (Fig. 4(e)). Owing to the design of the resonance structure, when the same output of the TENG is applied as a

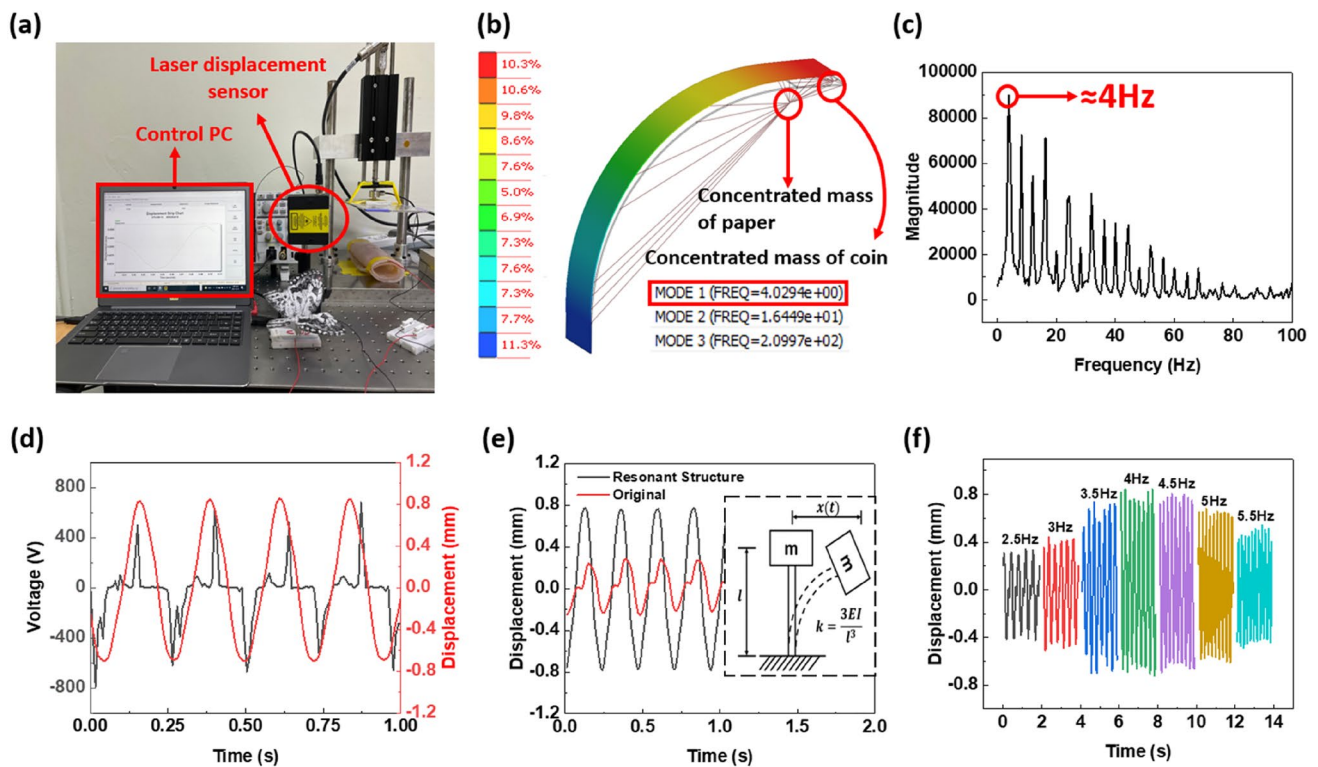


Fig. 4 Butterfly wing movement experiment; **a** butterfly wing displacement measurement setup using laser displacement sensor; **b** resonant frequency analysis of resonant structure through modal analysis; **c** frequency response characteristics of TENG output through

Fast Fourier Transform; **d** butterfly wing displacement in response to TENG output; **e** displacement difference analysis between the resonance structure and the original structure; **f** displacement difference at different frequencies acting on the resonant structure

power source, the natural frequency of the butterfly matches the output frequency of the TENG; therefore, the driving displacement of the butterfly wing is increased because of the resonance phenomenon. We analyzed the displacement difference based on the frequency acting on the soft robot (with the resonance structure design) (Fig. 4(f)). The resonance structure was designed to generate resonance at 4 Hz to respond to low-frequency naturally occurring mechanical stimuli. The experiment was conducted at a frequency range of 2.5–5.5 Hz. The maximum displacement was observed at the resonance frequency of 4 Hz. However, the displacement decreased when the frequency was lower or higher than 4 Hz (Fig. 4(f)).

The second insect-mimicking artificial robot was an inch-worm-type soft robot. Inch-worms perform forward motion by repeating the body bending and stretching processes. The PVDF film inch-worm simulates forward motion by using the characteristic that bending and stretching occur depending on the polarity of the applied input voltage. To make an effective forward motion, it is important to make one large bending, so a high single peak voltage is required. In order to obtain the required output performance, a self-made large-area TENG tester and a larger-area TENG specimen were used (Fig. 5(a)). The large-area TENG tester operates by

fixing one edge of the TENG specimen, lifting the opposite edge at an angle of 60° , and striking the floor again. The TENG can be driven in contact-separation mode using this equipment, and output of up to 1200 V and 25 μA could be obtained (Fig. 5(b) and (c)). To drive the PVDF film, it is essential to apply a high voltage to obtain the maximum speed; it is important to find the optimal structure through the kinematic design. Five parameters affecting the forward speed were set, and the optimal parameter design method was used to design the structure of the inch-worm (Fig. 5(d)).

The five parameters L_1 , L_2 , θ , μ_1 , and μ_2 are the hind leg length, forelimb length, forelimb angle, and the friction coefficient applied to the hind leg and forelimb pad, respectively. Based on experiments, the optimal design variable values were set as $L_1 = 30$ mm, $L_2 = 20$ mm, $\theta = 120^\circ$, $\mu_1 = 0.7$, $\mu_2 = 0.05$. The fastest moving speed was measured at 1.64 m/h (Fig. 5(e)). The maximum forward speed was obtained, based on the optimal parameter design method, when the ratio of the length of the hind leg (L_1) to the length of the forelimb (L_2) was 1.5:1. The movement mechanism of the inch-worm was classified into three stages, and the motion deformation of the hind leg and forelimb occurring in each stage was analyzed (Fig. 5(f)). The locomotion

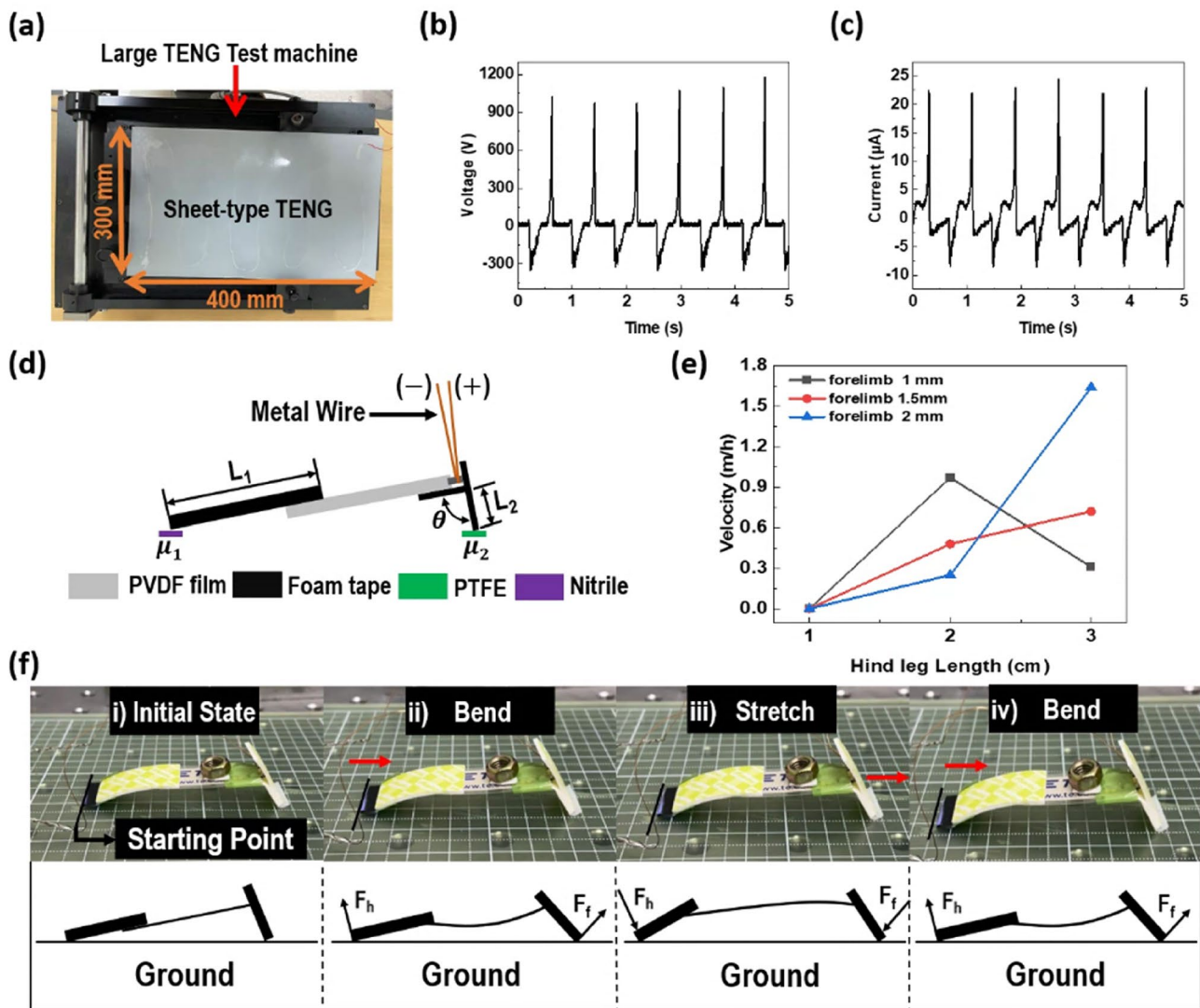


Fig. 5 Inch-worm drive test; **a** large-area TENG experimental setup for driving PVDF film inch-worm soft robot; **b–c** output voltage and output current, respectively; **d** inch-worm structure (optimal param-

eter designed); **e** speed comparison result using optimal design; **f** inch-worm forward drive mechanism

mechanism of the inch-worm was divided into three types: (i) initial state, (ii) bend state, (iii) stretch state. In the initial state (Fig. 5(f (i))), there is no change in the movement of the inch-worm soft robot because the electric output of the TENG is not applied robot. In the bend state (Fig. 5(f (ii))), a voltage in the anode direction of the TENG is applied to the PVDF film, causing the PVDF film to bend downward. The positional deformation of the hind leg and forelimb occur according to the deformation of the PVDF film. We analyzed the movement by vector decomposition of the reaction force generated between the support point of each leg and the support surface. The magnitude of the force acting vertically was larger than the magnitude of the force acting horizontally in the reaction force generated in the hind leg. The inch-worm soft robot was prevented from being

pushed back by using nitrile rubber with a large friction factor as a pad. The forelimb generated a reaction force due to the PVDF film deformation. However, the lateral force was larger than the vertical force, causing the forelimb to move forward. In addition, the pad of the forelimb used a PTFE film with a low friction factor to slide smoothly forward (Supplementary Fig. S2(a), movies S2 and S3). In the stretch state (Fig. 5(f (iii))), the cathode voltage of the TENG is applied to the PVDF film, resulting in upward bending deformation. In the forelimb, the magnitude of the force acting in the vertical direction is greater than that of the force in the horizontal direction, and the forward motion does not occur. However, the hind leg is pulled in the forward direction because the force in the horizontal direction is greater than the force in the vertical direction (Supplementary

Fig. S2(b)). By repeating this process, we obtained a speed of about 1.64 m/h. These results demonstrate that a soft robot fabricated using PVDF film can be driven using the resonance design and parameter design methods.

4 Conclusions

In this study, a TENG that converts external vibration or kinetic energy into electrical energy was developed and used to power a PVDF film-based insect-simulating soft robot. Other energy harvesting techniques are not suitable for driving PVDF film actuators owing to their low output voltage. However, because a TENG outputs high voltage, it can efficiently and directly apply power to the PVDF film without using rectifiers or transformation circuits. In addition, we used a resonance structure parameter design to amplify the small displacement of the PVDF film actuator. The results of the butterfly-wing experiment demonstrate that the driving displacement increased by approximately 2.5 times. Furthermore, we fabricated an inch-worm-type soft robot using the optimal parameter design method. The PVDF film actuator was controlled by the output of the TENG to create forward motion utilizing the bending phenomenon. The inch-worm soft robot could advance at a speed of up to 1.64 m/h, which proves that it can be used as a robot that can autonomously operate without a battery by controlling the input of the TENG. This study provides design guidelines that can effectively increase the movement of soft robots through optimal parameter design and resonance design, based on the presented experimental analysis. In the future, if the low current of the TENG is supplemented, it is possible to create a larger movement; therefore, it is expected to be a useful solution to replace various equipment that requires the power of a soft robot.

Author contributions All authors contributed to the study. Conceptualization, methodology, writing—original draft, writing—review, and editing were performed by SJ. Methodology, writing—review, and editing were carried out by SJ and DHK. Experiment, writing—review, and editing were carried out by SJ, JS, JM, J-HY, and K-UK. The simulation, writing—review, and editing were performed by SJ, JY and HC. The validation, resources, writing—review, and editing were carried out by JP. All authors have read and agreed to the published version of the manuscript.

Funding This work was supported by the Education and Research promotion program of KOREATECH in 2021 and the Korea Medical Device Development Fund grant funded by the Korea government (the Ministry of Health & Welfare, Republic of Korea) (Project Number: KMDF_PR_20200901_0167) and “Regional Innovation Strategy (RIS)” through the National Research Foundation of Korea (NRF) funded by the Ministry of Education (MOE)(2022RIS-004) and Korea Institute for Advancement of Technology (KIAT) grant funded by the Korea Government (MOTIE) (P0008458, The Competency Development Program for Industry Specialist).

Declarations

Conflict of interest The authors declare no conflict of interest.

References

- Dong, W. T., Xiao, L., Hu, W., Zhu, C., Huang, Y. A., & Yin, Z. P. (2017). Wearable human-machine interface based on PVDF piezoelectric sensor. *Transactions of the Institute of Measurement and Control*, 39(4), 398–403. <https://doi.org/10.1177/0142331216672918>
- Near, C. D. (1996). Piezoelectric actuator technology. *Smart Structures and Integrated Systems*, 2717, 246–258. <https://doi.org/10.1117/12.239027>
- Seminara, L., Capurro, M., Cirillo, P., Cannata, G., & Valle, M. (2011). Electromechanical characterization of piezoelectric PVDF polymer films for tactile sensors in robotics applications. *Sensors and Actuators A: Physical*, 169(1), 49–58. <https://doi.org/10.1016/j.sna.2011.05.004>
- Tian, H. (2018). A robot attached the soft sensor using PVDF film for objects discrimination. *Integrated Ferroelectrics*, 192(1), 94–102. <https://doi.org/10.1080/10584587.2018.1521657>
- Ahmed, S., Ounaies, Z., & Lanagan, M. T. (2017). On the impact of self-clearing on electroactive polymer (EAP) actuators. *Smart Materials and Structures*. <https://doi.org/10.1088/1361-665X/aa87c7>
- Wax, S. G., & Sands, R. R. (1999). Electroactive polymer actuators and devices. *Smart Structures and Materials 1999: Electroactive Polymer Actuators and Devices*, 3669: 2–10. <https://doi.org/10.1117/12.349666>
- Madden, J. D. W., Vandesteeg, N. A., Anquetil, P. A., Madden, P. G. A., Takshi, A., Pytel, R. Z., Lafontaine, S. R., Wieringa, P. A., & Hunter, I. W. (2004). Artificial muscle technology: Physical principles and naval prospects. *Ieee Journal of Oceanic Engineering*, 29(3), 706–728. <https://doi.org/10.1109/Joe.2004.833135>
- Wu, Y. C., Yim, J. K., Liang, J. M., Shao, Z. C., Qi, M. J., Zhong, J. W., Luo, Z. H., Yan, X. J., Zhang, M., Wang, X. H., Fearing, R. S., Full, R. J., & Lin, L. W. (2019). Insect-scale fast moving and ultrarobust soft robot. *Science Robotics*. <https://doi.org/10.1126/scirobotics.aax1594>
- Fan, F.-R., Tian, Z.-Q., & Wang, Z. L. (2012). Flexible triboelectric generator. *Nano Energy*, 1(2), 328–334. <https://doi.org/10.1016/j.nanoen.2012.01.004>
- Ghaderiaram, A., Bazrafshan, A., Firouzi, K., & Kolahdouz, M. (2021). A multi-mode R-TENG for self-powered anemometer under IoT network. *Nano Energy*. <https://doi.org/10.1016/j.nanoen.2021.106170>
- Qiu, C., Wu, F., Shi, Q., Lee, C., & Yuce, M. R. (2019). Sensors and control interface methods based on triboelectric nanogenerator in IoT applications. *Ieee Access*, 7, 92745–92757. <https://doi.org/10.1109/ACCESS.2019.2927394>
- Li, J., Wu, C., Dharmasena, I., Ni, X., Wang, Z., Shen, H., Huang, S.-L., & Ding, W. (2020). Triboelectric nanogenerators enabled internet of things: A survey. *Intelligent and Converged Networks*, 1(2), 115–141. <https://doi.org/10.23919/ICN.2020.0008>
- Wang, Y., Liu, X. Y., Wang, Y. W., Wang, H., Wang, H., Zhang, S. L., Zhao, T. C., Xu, M. Y., & Wang, Z. L. (2021). Flexible Seaweed-Like Triboelectric Nanogenerator as a Wave Energy Harvester Powering Marine Internet of Things. *ACS Nano*, 15(10), 15700–15709. <https://doi.org/10.1021/acsnano.1c05127>
- Liu, L., Shi, Q. F., Ho, J. S., & Lee, C. (2019). Study of thin film blue energy harvester based on triboelectric nanogenerator and seashore IoT applications. *Nano Energy*. <https://doi.org/10.1016/j.nanoen.2019.104167>

15. Mathew, A. A., Chandrasekhar, A., & Vivekanandan, S. (2021). A review on real-time implantable and wearable health monitoring sensors based on triboelectric nanogenerator approach. *Nano Energy*, 80, 105566. <https://doi.org/10.1016/j.nanoen.2020.105566>
16. Zheng, Q., Shi, B., Fan, F., Wang, X., Yan, L., Yuan, W., Wang, S., Liu, H., Li, Z., & Wang, Z. L. (2014). In vivo powering of pacemaker by breathing-driven implanted triboelectric nanogenerator. *Advanced Materials*, 26(33), 5851–5856. <https://doi.org/10.1002/adma.201402064>
17. Zheng, Q., Zou, Y., Zhang, Y. L., Liu, Z., Shi, B. J., Wang, X. X., Jin, Y. M., Ouyang, H., Li, Z., & Wang, Z. L. (2016). Biodegradable triboelectric nanogenerator as a life-time designed implantable power source. *Science Advances*. <https://doi.org/10.1126/sciadv.1501478>
18. Hinchet, R., Yoon, H. J., Ryu, H., Kim, M. K., Choi, E. K., Kim, D. S., & Kim, S. W. (2019). Transcutaneous ultrasound energy harvesting using capacitive triboelectric technology. *Science*. <https://doi.org/10.1126/science.aan3997>
19. Gunawardhana, K. S. D., Wanasekara, N. D., & Dharmasena, R. I. G. (2020). Towards truly wearable systems: Optimising and scaling up wearable triboelectric nanogenerators. *Isience*. <https://doi.org/10.1016/j.isci.2020.101360>
20. Pan, C. F., Liu, D. Y., Ford, M. J., & Majidi, C. (2020). Ultrasound-stretchable, Wearable Triboelectric Nanogenerator Based on Sedimented Liquid Metal Elastomer Composite. *Advanced Materials Technologies*. <https://doi.org/10.1002/admt.202000754>
21. Zhou, T., Zhang, C., Han, C. B., Fan, F. R., Tang, W., & Wang, Z. L. (2014). Woven Structured Triboelectric Nanogenerator for Wearable Devices. *Acs Applied Materials & Interfaces*, 6(16), 14695–14701. <https://doi.org/10.1021/am504110u>
22. Mule, A. R., Dudem, B., Graham, S. A., & Yu, J. S. (2019). Humidity sustained wearable pouch-type triboelectric nanogenerator for harvesting mechanical energy from human activities. *Advanced Functional Materials*, 29(17), 1807779. <https://doi.org/10.1002/adfm.201807779>
23. Jang, S., et al. (2019). Optimization of electrospinning parameters for electrospun nanofiber-based triboelectric nanogenerators. *International Journal of Precision Engineering and Manufacturing-Green Technology*, 6(4), 731–739. <https://doi.org/10.1007/s40684-019-00134-0>
24. Khalid, S., et al. (2019). A review of human-powered energy harvesting for smart electronics: Recent progress and challenges. *International Journal of Precision Engineering and Manufacturing-Green Technology*, 6, 821–851. <https://doi.org/10.1007/s40684-019-00144-y>
25. Shahriar, M., Vo, C. P., & Ahn, K. K. (2019). Self-powered flexible PDMS channel assisted discrete liquid column motion based triboelectric nanogenerator (DLC-TENG) as mechanical transducer. *International Journal of Precision Engineering and Manufacturing-Green Technology*, 6(5), 907–917. <https://doi.org/10.1007/s40684-019-00148-8>
26. Kim, K., & Yun, K.-S. (2019). Stretchable power-generating sensor array in textile structure using piezoelectric functional threads with hemispherical dome structures. *International Journal of Precision Engineering and Manufacturing-Green Technology*, 6(4), 699–710. <https://doi.org/10.1007/s40684-019-00127-z>
27. Lee, D., et al. (2019). A deformable foam-layered triboelectric tactile sensor with adjustable dynamic range. *International Journal of Precision Engineering and Manufacturing-Green Technology*, 6(1), 43–51. <https://doi.org/10.1007/s40684-019-00024-5>
28. Kim, J., Cho, H., Han, M., Jung, Y., Kwak, S. S., Yoon, H. J., Park, B., Kim, H., Kim, H., Park, J., & Kim, S. W. (2020). Ultra-high Power Output from Triboelectric Nanogenerator Based on Serrated Electrode via Spark Discharge. *Advanced Energy Materials*. <https://doi.org/10.1002/aenm.202002312>
29. Xiang, C., et al. (2017). The design, hysteresis modeling and control of a novel SMA-fishing-line actuator. *Smart Materials and Structures*, 26(3), 037004. <https://doi.org/10.1088/13610665X/aa5b03>
30. Bar-Cohen, Y., & Anderson, I. A. (2019). Electroactive polymer (EAP) actuators—background review. *Mechanics of Soft Materials*, 1(1), 1–14. <https://doi.org/10.1007/s42558-019-0005-1>
31. Sun, W., et al. (2021). TENG-Bot : Triboelectric nanogenerator powered soft robot made of uni-directional dielectric elastomer. *Nano Energy*, 85, 106012. <https://doi.org/10.1016/j.nanoen.2021.106012>

Publisher's Note Springer Nature remains neutral with regard to jurisdictional claims in published maps and institutional affiliations.

Springer Nature or its licensor (e.g. a society or other partner) holds exclusive rights to this article under a publishing agreement with the author(s) or other rightsholder(s); author self-archiving of the accepted manuscript version of this article is solely governed by the terms of such publishing agreement and applicable law.



Sungho Ji received his B.S. degree from Kongju National University of Engineering, Cheonan, Republic of Korea, in 2021. He is currently an M.S. candidate at Korea University of Technology and Education, Cheonan, Republic of Korea. His current research interests include triboelectric energy harvesting for various mechanical energy applications.



Jaehee Shin received her B.S. degree from Kongju National University of Engineering, Cheonan, Republic of Korea, in 2020. She is currently an M.S. candidate at Korea University of Technology and Education, Cheonan, Republic of Korea. Her current research interests include triboelectric energy harvesting for various mechanical energy applications.



Jiyoung Yoon received her M.S. degree from the Korea Advanced Institute of Science and Technology (KAIST), Daejeon, Republic of Korea, in 2007. She is currently a researcher at Advanced Mechatronics R&D Group, Korea Institute of Industrial Technology. Her research interests include the modeling and simulation of multiphysics systems.

neering and the Director of the Human–Robot Interaction Laboratory, KAIST.



Duck Hwan Kim received a Ph.D. from Korea University, Seoul, Republic of Korea, in 2009. He has been working as a researcher at SAMSUNG Research Seoul R&D Group.



Jung-Hwan Youn received his M.S. degree in mechanical engineering from the Yonsei University, Seoul, South Korea, in 2018. He is currently pursuing his Ph.D. in mechanical engineering from the Korea Advanced Institute of Science and Technology (KAIST), Daejeon, Republic of Korea. In 2018, he joined the Human–Robot Interaction Laboratory, KAIST. His research interests include soft robotics, micro robotics, and haptics.



Hanchul Cho has received Ph.D. degree from Northeastern University in the USA in 2014. He has been working as a principle researcher at Korea Institute of Industrial Technology since 2015. His research is interested in physical sensors and triboelectric nanogenerator.



Jihyeong Ma received his B.S. degree from Sungkyunkwan University, Suwon, Republic of Korea, in 2019, and M.S. degree from the Korea Advanced Institute of Science and Technology (KAIST), Daejeon, Republic of Korea, in 2021. He is currently pursuing his Ph.D. in mechanical engineering from the Korea Advanced Institute of Science and Technology (KAIST), Daejeon, Republic of Korea. In 2019, he joined the Human–Robot Interaction Laboratory, KAIST. His research interests



Jinhyoung Park received a B.S., M.S., and Ph.D. from the Korea Advanced Institute of Science and Technology (KAIST), Daejeon, Republic of Korea, in 2003, 2005, and 2009, respectively. He is currently a professor at the School of Mechatronics Engineering, Korea University of Technology and Education. His research interests include high-voltage application of a triboelectric nanogenerator.

include triboelectric nanogenerators and soft robotics.



Ki-Uk Kyung received his bachelor's and Ph.D. degrees in mechanical engineering from the Korea Advanced Institute of Science and Technology (KAIST), Daejeon, South Korea, in 1999 and 2006, respectively. In 2006, he joined the POST PC Research Group, Electronics and Telecommunications Research Institute, Daejeon, where he is currently the Director of the Smart UI/UX Device Research Section. Since 2018, he has been an Associate Professor of Mechanical Engi-